Contents lists available at ScienceDirect

Arabian Journal of Chemistry

Original article

Utilization of landscape biomass waste as activated carbon to scavenge oxytetracycline: Attraction mechanism, batch and continuous studies

Mohamad Nasran Nasehir Khan [a], Mohamad Firdaus Mohamad Yusop [a],
Muhamad Faizal Pakir Mohamed Latiff [b], Mohd Azmier Ahmad [a,*]

[a] *School of Chemical Engineering, Engineering Campus, Universiti Sains Malaysia, 14300 Nibong Tebal, Penang, Malaysia*
[b] *Civil Engineering Studies, College of Engineering, Universiti Teknologi MARA, Permatang Pauh Campus, 13500 Permatang Pauh, Penang, Malaysia*

ARTICLE INFO

ABSTRACT

Oxytetracycline (OXY) is an antibiotic widely used in the livestock industry and its existence in water can cause antibiotic resistance genes. A treatment process in a continuous mode is required to treat a high volume of OXY wastewater. Hence, an effort was made in this study to adsorb OXY from an aqueous solution (batch and continuous modes) using landscape biomass waste-based activated carbon (LBWAC). This adsorbent was produced via potassium hydroxide (KOH) chemical treatment combined with microwave heating under carbon dioxide, CO_2 gas. The resulting LBWAC exhibited 973.21 m^2/g of BET surface area, 842.18 m^2/g of mesopores surface area, 0.3911 cm^3/g of total pore volume, and 2.44 nm of average pore diameter. In a batch study, OXY adsorption uptakes increased whilst OXY percentage removal decreased when OXY starting concentration increased from 25 to 300 mg/L. The highest uptakes of OXY occurred at a solution temperature of 60 °C (228.44 mg/g) and a solution pH of 12 (63.22 mg/g). The adsorption system studied obeyed the Langmuir model and pseudo-second-order in isotherm and kinetic studies, respectively. The obtained Langmuir monolayer capacity, Q_m was 344.83 mg/g. Mechanism study revealed that O, H, and N elements in OXY molecules react with O, H, and N elements in functional groups on LBWAC's surface via hydrogen bonds and vice versa. Parameters acquired in the thermodynamic study described the adsorption process as spontaneous, endothermic, and physisorption-controlled. The continuous bed column study revealed that the breakthrough point (T_b), exhaustion time (T_{ex}), and maximum adsorption uptake (q_{max}) for the OXY-LBWAC adsorption system can be increased by decreasing the starting inlet concentration, decreasing the inlet flow rate and increasing the bed height. The continuous adsorption data fitted Thomas model the best. The LBWAC had a good potential to be applied in a large-scale operation for OXY wastewater treatment.

1. Introduction

Antibiotics are a class of medications used to treat bacterial infections. They work by killing or inhibiting the growth of bacteria, thus helping the body's immune system to eliminate the infection (Kovalakova et al., 2020). Antibiotics pose a significant environmental concern among the various pollutants, primarily due to their persistence and presence in drinking water, surface water, and wastewater, where their detection is frequent. The introduction of antibiotics has resulted in a growing pollution problem in aquatic environments, largely attributed to the improper use and overuse of pharmaceuticals in aquaculture, livestock farming, and hospital settings. Certain antibiotics exhibit limited oral bioavailability, resulting in their prolonged presence in the gastrointestinal tract beyond the desired duration. As a consequence, these antibiotics are excreted into the environment in residual and unabsorbed forms, potentially retaining their biological activity (Nkoh et al., 2023). One of the regular antibiotics that can be detected as a pollutant in water and soil is oxytetracycline (OXY) (Conde-Cid et al., 2019, Wang et al., 2023). OXY belongs to the category of tetracyclines, a class of broad-spectrum antibiotics extensively employed in the livestock industry. These antibiotics exhibit activity against various types of microorganisms, including

Production and hosting by Elsevier

Mohamad Nasran Nasehir Khan, Mohamad Firdaus Mohamad Yusop, Muhamad Faizal Pakir Mohamed Latiff et al.

Arabian Journal of Chemistry 16 (2023) 105256

numerous Gram-positive and Gram-negative bacteria (Zhang et al., 2023). In the future, the generation of wastewater containing antibiotics is expected to increase due to the increment of antibiotic usage worldwide due to (i) an increasing human population, (ii) easy access to antibiotics and (iii) increase demand for animal protein leads to an increase in antibiotics usage to sustain the food production (Van Boeckel et al., 2015, Zhao et al., 2019). Exposure to antibiotic residues causes a notable threat in terms of the rise of antibiotic-resistance genes and antibiotic-resistant bacteria (Zhan et al., 2020). Therefore, there is a need to develop an effective yet economical-friendly method to treat the ever-increasing wastewater containing antibiotics.

There are many methods to treat antibiotics wastewater. For instance, Cuerda-Correa et al. (2020) adopted advanced oxidation processes whilst Li et al., (2020) and Du et al., (2021) utilized photodegradation using metal–organic frameworks to treat antibiotics in wastewater. These methods are efficient but high in cost for chemical reagents or catalysts besides producing secondary pollutants in the form of metal sludge (Leng et al., 2020). Xiong et al., (2021), Ferrando and Matamoros (2020), and Gojkovic et al., (2019) studied algae-based techniques to treat antibiotics wastewater. Despite its effectiveness, this method requires relatively longer time to achieve its objective. In a study conducted by Bai and Acharya (2016), 7 days were needed to remove antibiotics from wastewater. Of all methods available, the adsorption process offers many advantages such as being effective, simple to operate, relatively fast process, and cheap (Mohamad Yusop et al., 2023a, 2023b, 2023c). Furthermore, this method has demonstrated versatility due to its ability to remove various type of contaminants from wastewater ranging from dyes (Lopes et al., 2021, Zhou et al., 2022, Zayed et al., 2023), heavy metals (Yusop et al., 2022a, 2022b, Bumajdad and Hasila 2023, Saka et al., 2023), water vapor (Liu et al., 2023), phenol (Arshad et al., 2019, Alam et al., 2023), nitric oxide (Lin et al., 2021), antibiotics (Zhou et al., 2022, Tiwari et al., 2023), hydrogen sulfide, H_2S gas (Moradi et al., 2020, Nor et al., 2021), and so on. One of the most effective adsorbents to be used in the adsorption process is activated carbon (AC). Researchers are actively producing AC from biomass wastes since they are free materials and renewable sources. For instance, edamame shell (He et al., 2023), coconut shell (Oyekanmi et al., 2019, Amran et al., 2021, Yusop et al., 2022a, 2022b), pineapple peel (Rosli et al., 2023), date seed (Said et al., 2023), wood wastes (Firdaus et al., 2022, Mohamad Yusop et al., 2023a, 2023b, 2023c), oak seeds (Borghei et al., 2021), mangosteen peel (Jawad et al., 2022), jackfruit peel (Mohamad Yusop et al., 2023a, 2023b, 2023c), orange peel (Ajay et al., 2021) and others. In this study, biomass waste from landscape tree (*Tabebuia rosea* tree) was selected as the precursor to be converted into activated carbon (AC). This tree is commonly known as "Malaysian Sakura" and is highly chosen as a landscaping plant. The local authorities in Malaysia have extensively planted this tree along roadsides, gardens, parks, residential areas, and university campuses (Nur et al., 2014). Despite its beauty, this tree has no other purposes and is often dumped in a dumping site. Therefore, utilizing their waste in AC would be beneficial in promoting the "waste to wealth" concept.

In the literature, few studies targeting OXY to be treated from wastewater were noticed. Nguyen et al., (2021) studied OXY adsorption by cobalt-based zeolite, Juengchareonpoon et al., (2019) utilized hydrogen film to adsorb OXY, and Khan et al., (2021) performed an adsorption test on OXY using groundwater treatment sludge as magnetic adsorbent. These studies share similarities in where the adsorption test was conducted through batch mode. The batch mode in the adsorption process is not suitable for large-scale applications due to (i) at the end of the adsorption process, the adsorbent is required to be filtered out from the solution, therefore adding more work and labour cost, (ii) variations in

terms pH and temperature occur in different batch, resulting inconsistencies in adsorption process and (iii) wasting adsorbent since adsorbent is used in excess quantity to achieve adequate adsorption. On the contrary, the continuous mode of adsorption process is more beneficial since it provides higher treatment capacity, improved efficiency, consistent performance, cost-effectiveness, control, and flexibility, making it a preferred choice for many large-scale or continuous treatment applications. Therefore, this research aimed to study the OXY adsorption onto LWBAC through batch and continuous bed column. The equilibrium, isotherm, kinetic, and thermodynamic studies were performed in batch adsorption whilst several adsorption models were utilized in continuous bed column to determine breakthrough time, T_b, and exhaustion time, T_{ex}. Moreover, the interaction between OXY molecules and LWBAC's surface was also verified to understand the adsorption mechanism involved. To the best of our knowledge, the investigation of antibiotic adsorption in a continuous bed column system and the possible OXY-LBWAC mechanism interaction is novel.

2. Materials and methods

2.1. Materials

The landscape biomass waste (*Tabebuia rosea* tree) was supplied by Seberang Perai City Council, Penang, Malaysia. Upon received, the size of this precursor was between 15- and 20-mm. Riedel-el Haen, Germany had supplied potassium hydroxide (KOH) to be utilized during chemical activation whereas Merck, Germany had provided hydrochloric acid, HCl to be used during the washing step. Both nitrogen, N_2 gas (consumed as an inert gas during char production in a vertical furnace) and carbon dioxide, CO_2 gas (utilized during microwave heating to provide gasification treatment on samples) were acquired from MOX Gases Berhad, Malaysia.

2.2. LBWAC preparation

The precursor was dried under direct sunlight in an open area for 72 h. 200 g of dried precursor was carbonized in a vertical furnace for 1 h at a carbonization temperature of 550 °C. The N_2 gas was purged through the vertical furnace at 150 cm³/min during the whole carbonization process. After 1 h, the furnace was turned off to lower the temperature of the sample to room temperature. The N_2 gas was allowed to purge through the furnace throughout the cooling process. Once the furnace reached room temperature, the sample was unloaded from the furnace. This sample is now known as char. The resulting char was impregnated with KOH at impregnation ratio (IR) of 1.00 g/g. IR is computed using Eq. (1):

$$IR = \frac{W_{KOH}}{W_{char}} \tag{1}$$

where W_{KOH} denotes the mass of KOH (g) while W_{char} refers to the mass of LBWAC. The chemical activation process took 24 h to complete. The impregnated char was then heated in a modified microwave oven (EMM2001W, Sweden) at 700 Watt for 20 min. The CO_2 gas purged through the quartz glass inside the microwave to provide a gasification effect on the sample. The resulting sample was washed with 0.1 M HCl solution until the pH of the washing solution became 7–8. The wet LBWAC was dried in an oven for 24 h. Dried LBWAC was kept in an air-tight container.

2.3. Methods of characterization

This study provides several characteristics for the samples produced. The first characterization of surface area (BET and meso-

Mohamad Nasran Nasehir Khan, Mohamad Firdaus Mohamad Yusop, Muhamad Faizal Pakir Mohamed Latiff et al.

Arabian Journal of Chemistry 16 (2023) 105256

pores), volume of total pores, and average diameter of the pores were acquired from Micromeritics volumetric adsorption analyser (ASAP 2010) (Baruah et al., 2022, Karakehya 2023). The characterization in terms of elemental composition and proximate composition was done by operating the elemental analyzer (Model: Perkin Elmer Series II 2400, USA) and simultaneous thermal analyzer (STA) (Model: Perkin Elmer STA 6000, USA), respectively (Askaruly et al., 2023). For quality control, the elemental analyzer is calibrated regularly using certified reference materials to ensure a precise measurement by linking the instrument's response to the element concentrations in the samples. The morphology image of samples was taken by scanning electron microscopy (SEM) was taken by (Model: LEO SUPRA 55VP, Germany) (Zayed et al., 2023). The zeta potential value was measured using the zeta potential analyser (Zetasizer Nano Series DKSH) (Senol-Arslan et al., 2022). The functional groups on samples were verified using Fourier transforms infrared spectroscopy (FTIR) (Model: Shidmazu Prestige 21, Japan), through the transmission method (Mawhinney and Yates 2001, Ahmad et al., 2020a, 2020b).

2.4. Preparation of OXY stock solution

To prepare the OXY solution, 1.00 g of accurately weighted OXY powder was mixed with 1 L of deionized water in a conical flask. The solution was stirred to dissolve the OXY powder completely. The resulting solution was known as a stock solution with a concentration of 1000 mg/L. To prepare the OXY solution at different initial concentrations, the stock solution was diluted using the following formula:

$$M_1 V_1 = M_2 V_2 \tag{2}$$

where M_1 and V_1 refer to the concentration and volume of stock solution used, respectively, whilst M_2 and V_2 refer to the concentration and volume of desired diluted solution, respectively.

2.5. Study of equilibrium

The influences of several factors on the equilibrium state of the adsorption process were verified. The first factor was starting concentration of the OXY solution. OXY solution with six different starting concentrations (25, 50, 100, 200, 250, and 300 mg/L) was prepared in an Erlenmeyer flask. The volume for each one of these solutions was 200 mL. These flasks were then inserted inside the water bath shaker, and 0.20 g of LBWAC was added to every flask. The rotating speed and temperature controller on the water bath shaker were set to 80 rpm and 30 °C, respectively. The second factor studied was the solution temperature effect. OXY starting concentration, OXY solution volume, LBWAC dosage and rotating speed were chosen to be 300 mg/L, 200 mL, 0.20 g, and 80 rpm, respectively, whilst the solution temperature was changed between 30, 45, and 60 °C. The third factor verified was the solution pH effect. The starting concentration for OXY was selected to be 100 mg/L and the pH of the OXY solution was altered using NaOH / HCl to be 2, 4, 6, 10, and 12. The measurement of pH was made using a pH meter (Model Delta 320, Mettler Toledo, China). Other experimental conditions followed the same conditions in the study for the solution temperature effect. At the equilibrium point (after 24 h), the concentration of OXY in the solution, C_e (Eq. (3)), and its percentage removal (Eq. (4)) are calculated using the following equations:

$$q_e = \frac{(C_o - C_e)V}{W} \tag{3}$$

$$\%Removal = \frac{C_o - C_e}{C_o} \times 100\% \tag{4}$$

where OXY starting concentration (mg/L), LBWAC weight used (g) and OXY solution volume (mL) were respectively denoted by C_o, W and V.

2.6. Study of isotherm

The data obtained in the equilibrium study were fitted on isotherm models namely Langmuir (Eq. (5)) (Langmuir 1918), Freundlich (Eq. (6)) (Freundlich 1906), and Temkin (Eq. (7)) (Tempkin and Pyzhev 1940). Their equations are as follows:

$$q_e = \frac{Q_m K_L C_e}{1 + K_L C_e} \tag{5}$$

$$q_e = K_F C_e^{\frac{1}{n_F}} \tag{6}$$

$$q_e = \frac{RT}{B} \ln(A C_e) \tag{7}$$

where maximum monolayer capacity (mg/g) and Langmuir constant related to adsorption capacity (L/mg) were represented by Q_m and K_L, respectively. The Freundlich constant related to adsorption strength $((mg/g)(L/mg)^{1/n})$ and heterogeneity factor (dimensionless) were denoted by K_F and n_F, respectively, whilst A (L/mg) was Temkin constant and B (L/mg) was another Temkin constant that linked to the heat of sorption (Mohamad Yusop et al., 2023a, 2023b, 2023c). Microsoft Excel Solver version 2016 was utilized to solve the non-linear equation of isotherm models to obtain the constants.

2.7. Study of kinetic

In contrast with equilibrium and isotherm studies, the study of kinetic was performed by measuring the concentration of OXY at a specific time interval between 0.15 h and 24 h. Other procedures in the kinetic study were similar to equilibrium and isotherm studies. The data obtained were tested on pseudo-first order, PFO (Eq. (8)) (Lagergren, 1898), and pseudo-second order, PSO (Eq. (9)) (Ho and McKay 1998). The rate-limiting step was determined from the Boyd plot (Eq. (10)) (Boyd et al., 1947). Their equations are as follows:

$$\ln(q_e - q_t) = \ln q_e - k_1 t \tag{8}$$

$$\frac{t}{q_t} = \frac{1}{k_2 q_e^2} + \frac{t}{q_e} \tag{9}$$

$$B_t = -0.4977 - \ln\left(1 - \frac{q_t}{q_e}\right) \tag{10}$$

where PFO's rate constant and PSO's rate constant are respectively denoted by k_1 and k_2 whilst B_t refers to Boyd number. The most suitable model for the isotherm and kinetic data was selected based on the R^2 value.

2.8. Study of thermodynamic

Two important parameters in thermodynamic study namely enthalpy change, $\Delta H°$ (kJ/mol), and entropy change $\Delta S°$ (kJ/mol. K) can be calculated from Van't Hoff equation (Eq. (12)) (Achmad et al., 2012) as follows:

$$lnK_c = \frac{\Delta S°}{R} - \frac{\Delta H°}{RT} \tag{11}$$

where R (8.314 J/mol.K) and T (K) are the gas constant and absolute temperature, respectively. The K_c (dimensionless) refers to the equi-

Mohamad Nasran Nasehir Khan, Mohamad Firdaus Mohamad Yusop, Muhamad Faizal Pakir Mohamed Latiff et al.

Arabian Journal of Chemistry 16 (2023) 105256

librium constant and can be determined as follows (Lima et al., 2019):

$$K_c = \frac{1000 \frac{mg}{g} \times K_L \times molecular\ weight\ of\ adsorbate\ \times\ [adsorbate]^\circ}{\gamma}$$

(12)

where $[adsorbate]^\circ$ can be simplified as 1 mol/L at standard state, Υ (dimensionless) represents the coefficient for the adsorbate activity whereas K_L (L/mg) refers to Langmuir constant. Another two thermodynamic parameters namely Gibbs free energy, ΔG° (kJ/mol) and activation energy, E_a (kJ/mol) can be found by using Eqs. (14) and (15), respectively:

Table 1
Physical properties of the samples.

Sample	BET surface area (m^2/g)	Mesopores surface area (m^2/g)	Total pore volume (cm^3/g)	Average pore diameter (nm)
precursor	0.98	–	0.0001	1.48
char	406.52	337.85	0.1586	1.75
LBWAC	973.21	842.18	0.3911	2.44

Table 2
Chemical composition of samples.

Samples	Proximate analysis (%)				Elemental analysis (%)			
	Moisture	Volatile matter	Fixed carbon	Ash	C	H	S	(N + O)
Precursor	13.05	58.22	22.85	5.88	41.45	10.11	0.12	48.32
Char	5.89	35.78	54.22	4.11	64.21	8.21	0.09	27.49
LBWAC	2.89	17.21	78.14	1.76	81.24	7.14	0.07	11.55

(a) (b)
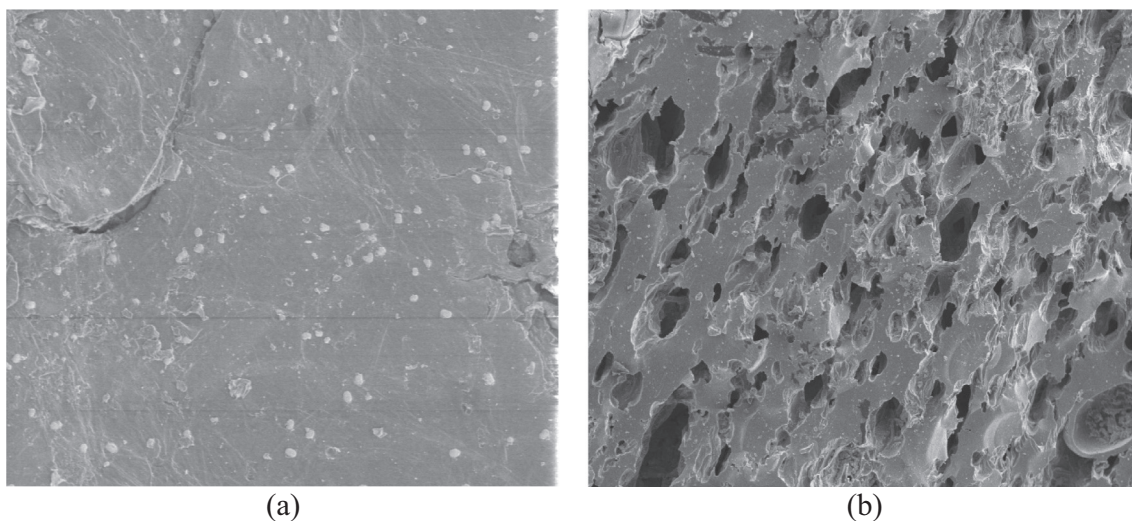
Fig. 1. SEM images of (a) precursor (b) LWBAC (1000x magnificent level).
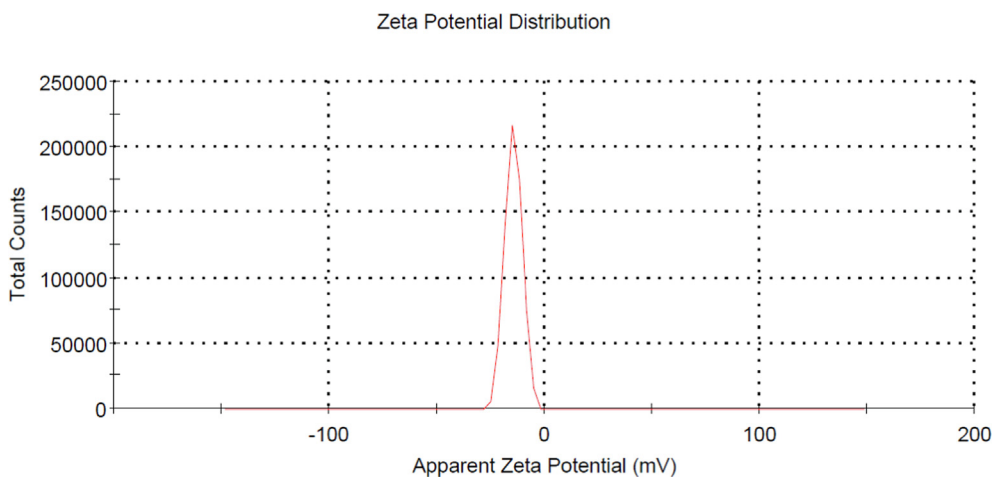
Fig. 2. Zeta potential value for LBWAC.

$$\Delta G^\circ = \Delta H^\circ - T\Delta S^\circ \tag{13}$$

$$lnk_2 = lnA - \frac{E_a}{RT} \tag{14}$$

where k_2 is PSO's rate constant and A refers to Arrhenius factor.

2.9. Study of continuous bed column

The effects of (i) starting influent concentration (50, 100, and 200 g/L), (ii) influent flow rate (10, 20, and 30 mL/min) and (iii) LBWAC bed height (40, 60, and 80 mm) on the continuous adsorption performance were investigated. A Perspex filter column with an internal diameter of 2.50 cm was used for this experiment. The OXY solution was pumped to the influent point using a peristaltic pump. A breakthrough curve was constructed by plotting the ratio of OXY concentration at time t to the OXY starting concentration (C_t/C_o) against contact time. Based on the breakthrough curve, the breakthrough time, T_b, and the exhaustion time, T_{ex} can be found at $0.10C_t/C_o$ and $0.90C_t/C_o$, respectively.
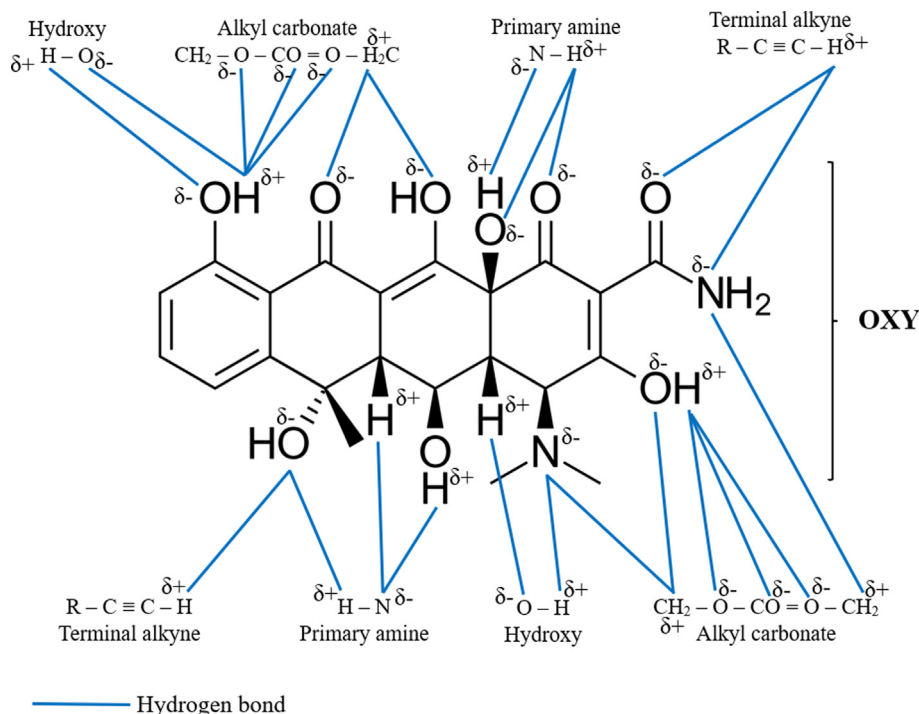
Fig. 3. Possible attraction mechanism between OXY molecules and functional groups on LBWAC's surface.
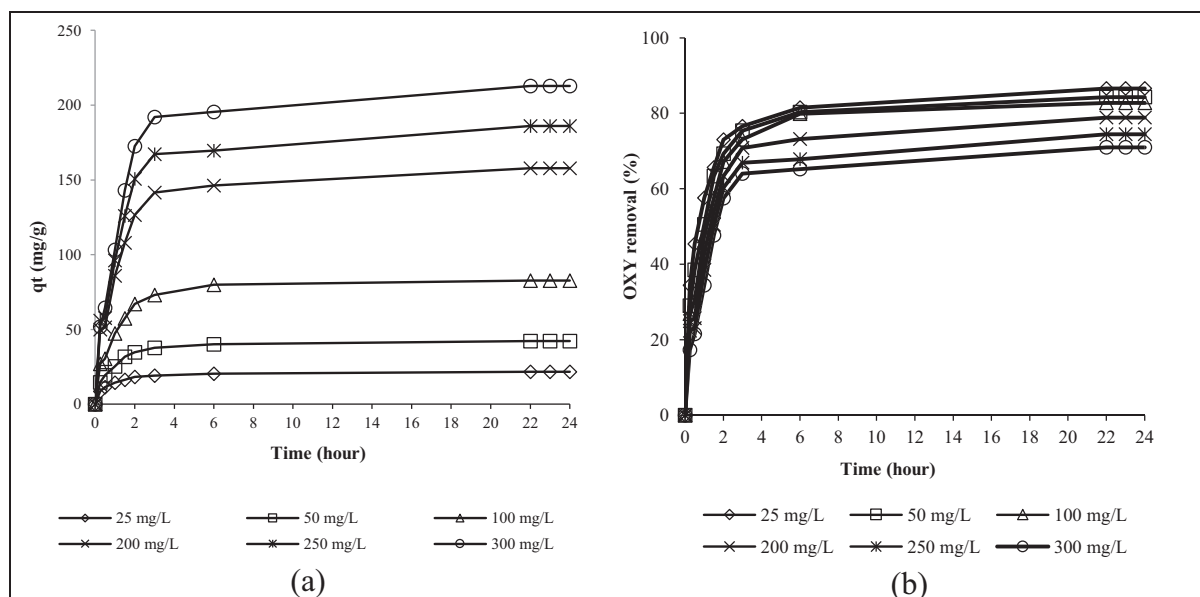
Fig. 4. ots of (a) adsorption uptakes by LBWAC versus time and (b) percentage removal by LBWAC versus time for different starting concentrations of OXY at 30 °C (weight of LWBAC was 0.2 g, volume solution of 200 mL and original pH were used).

5
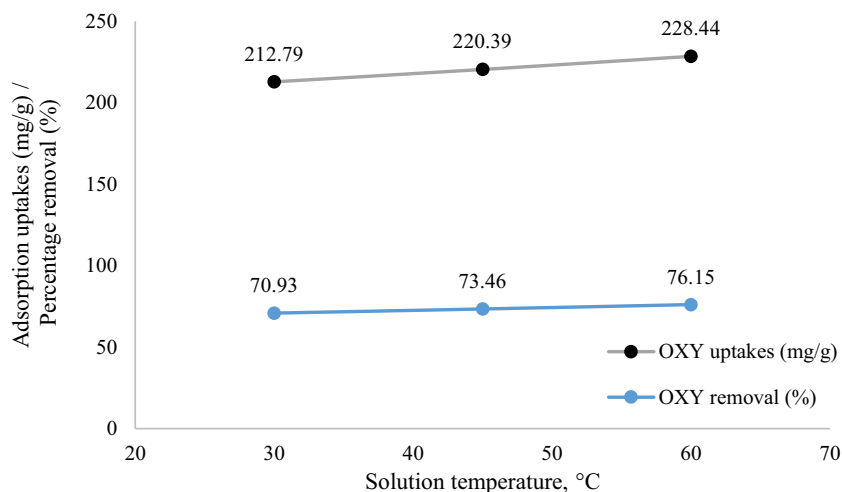
Fig. 5. Plot of adsorption capacity at different solution temperature (weight of LWBAC was 0.2 g, volume solution of 200 mL, initial concentration of 300 mg/L and original pH).

3. Results and discussions

3.1. Characteristics of samples

Table 1 provides the physical properties of the samples studied. The carbonization process succeeded in initializing the pores development process in the precursors. Therefore, the resulting char exhibited 406.52 m^2/g of BET surface area, 337.85 m^2/g of mesopores surface area, 0.1586 cm^3/g of pore volume, and an average pore diameter of 1.75 nm. These properties were noticed to increase further owing to an effective activation process that combined KOH chemical treatment, microwave heating, and CO_2 gasification treatment. During these activation processes, the following chemical reaction took place (Norouzi et al., 2018, Xu et al., 2019, Mohamad Yusop et al., 2023a, 2023b, 2023c):

$$2KOH \text{ (aq)} \rightarrow K_2O \text{ (s)} + H_2O \text{ (l)} \quad (15)$$

$$H_2O \text{ (l)} + C \text{ (s)} \rightarrow CO \text{ (g)} + H_2 \text{ (g)} \quad (16)$$

$$CO \text{ (g)} + H_2O \text{ (l)} \rightarrow CO_2 \text{ (g)} + H_2 \text{ (g)} \quad (17)$$

$$CO_2 \text{ (g)} + K_2O \text{ (s)} \rightarrow K_2CO_3 \text{ (s)} \quad (18)$$

$$K_2CO_3 \text{ (s)} \rightarrow K_2O \text{ (s)} + CO_2 \text{ (g)} \quad (19)$$

$$CO_2 \text{ (g)} + C \text{ (s)} \rightarrow 2CO \text{ (g)} \quad (20)$$

$$K_2O \text{ (s)} + 2C \text{ (s)} \rightarrow K \text{ (s)} + 2CO \text{ (g)} \quad (21)$$

$$K_2CO_3 \text{ (s)} + C \text{ (s)} \rightarrow 2 \text{ K (s)} + 3CO \text{ (g)} \quad (22)$$
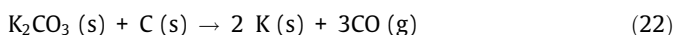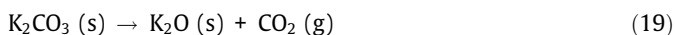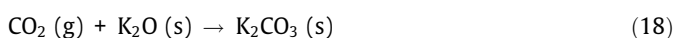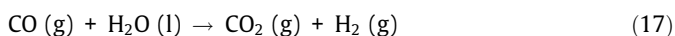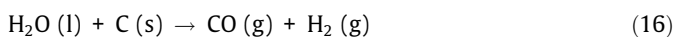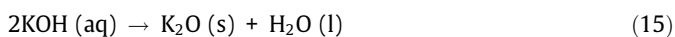
The K_2CO_3 ions penetrate the internal side of the sample whilst the microwave heating promoted more volatile matter to erupt and leave the sample. This led to the increment of BET surface area, mesopores surface area, and total pore volume in LBWAC to be 973.21 m^2/g, 842.18 m^2/g, and 0.3911 cm^3/g, respectively. The gasification effect of CO_2 aided the pores enlargement process, thus converting the micropores in char to mesopores (2.44 nm) in LBWAC.

Table 2 presents the chemical composition of the samples. Based on the proximate analysis, the precursor used in this study posed 22.85% of fixed carbon content which is higher in comparison to pomegranate fruit peel of 15.34% (Ahmad et al., 2020a,

2020b), and durian peel at 20.69% (Yusop et al., 2021). A high fixed carbon percentage is good since it made up the matrix structure of adsorbent A higher percentage of fixed carbon is usually linked to a finely developed porous arrangement. The empty spaces and gaps present in AC create a generous expanse of surface, enabling the adsorption process. Elevated fixed carbon levels frequently signify an increased volume of accessible pore areas, resulting in an
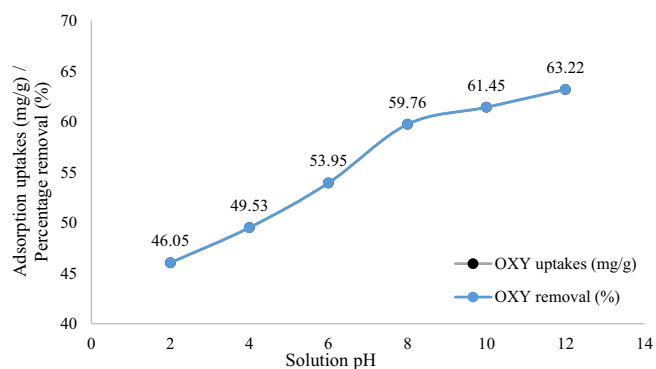
Fig. 6. Percentage removal of adsorbates by LBWAC versus solution pH (weight of LWBAC was 0.2 g, volume solution of 200 mL, initial concentration of 100 mg/L and solution temperature of 30 °C).
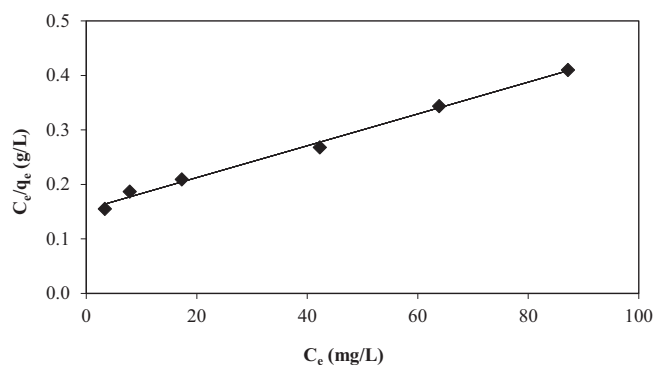
Fig. 7. Langmuir isotherm plot for OXY-LBWAC adsorption system at 30 °C (weight of LWBAC was 0.2 g, volume solution of 200 mL and original pH were used).

Mohamad Nasran Nasehir Khan, Mohamad Firdaus Mohamad Yusop, Muhamad Faizal Pakir Mohamed Latiff et al.

Arabian Journal of Chemistry 16 (2023) 105256
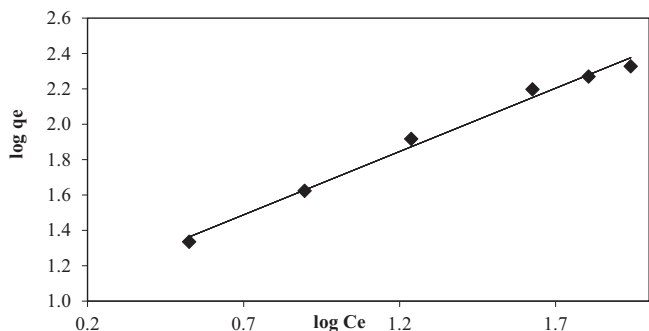
Fig. 8. Freundlich isotherm plot for OXY-LBWAC adsorption system at 30 °C (weight of LWBAC was 0.2 g, volume solution of 200 mL and original pH were used).
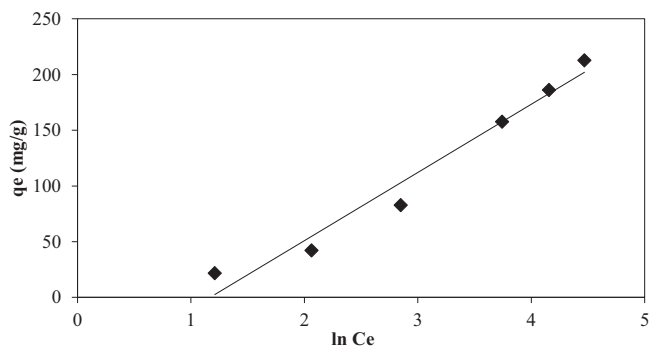
Fig. 9. Temkin isotherm plot for OXY-LBWAC adsorption system at 30 °C (weight of LWBAC was 0.2 g, volume solution of 200 mL and original pH were used).

Table 3
Isotherm parameters for OXY-LBWAC adsorption system at 30 °C.

Isotherms	Parameters	
Langmuir	Q_m (mg/g)	344.83
	K_L (L/mg)	0.0188
	R^2	0.9939
Freundlich	n_F	1.40
	K_F $(mg/g)(L/mg)^{1/n}$	9.72
	R^2	0.9906
Temkin	B_T (kJ)	61.24
	A_T (L/mg)	0.31
	R^2	0.9664

expanded surface region. This expansion, in turn, facilitates the creation of additional sites for adsorption to take place (Firdaus et al., 2022). Carbonization and activation processes caused a further increment of fixed carbon percentage in LBWAC to 78.14%. Other components such as moisture and volatile matter shrink in percentage from 13.05% and 58.22% in precursor to 2.89% and 17.21% in LWBAC, respectively. These components evaporate and leave the sample. A relatively low ash percentage of 1.76% was good since ash contains ruptured pores, therefore is useless for the adsorption process. In terms of elemental composition, LWBAC was found to be dominated by C element (80.12%), followed by N + O elements (12.48%), H element (7.14%), and S element (0.07%). The existence of N, O, and S elements in LBWAC gave an insight that this adsorbent is filled with various functional groups on its surface.

Fig. 1(a) and (b) respectively show the SEM image for precursor and LBWAC. The precursor surface was seen to be dense with no pores since the precursor is packed with lignin, cellulose, hemicellulose, and tar components. These components vaporized during the carbonization and activation process. Hence, a porous structure can be observed on LBWAC's surface. These porous structures were contributed by the penetration of K_2CO_3 during chemical.

The zeta potential of LBWAC was found to be −14.5 mV, as shown in Fig. 2. A negative value of zeta potential signified that the LBWAC's surface was negatively charged due to the existence of functional groups such as hydroxyl and carboxyl. The FTIR analysis shows that the surface of the precursor was filled with functional groups of vinyl C—H out-of-plane bend, primary amine C—N stretch, aryl -O stretch, methylene C—H asymmetric and alkyne C—H stretch at peaks of 890, 1030 & 1627, 1251, 2915 and 3320 cm^{-1}, respectively. Only the primary amine C—N stretch survived the activation processes and appeared in LBWAC's at 1076 cm^{-1}, whilst other functional groups were missing in LBWAC's surface. Several new peaks representing new functional groups were formed on LBWAC's surface. These new functional groups include alkyl carbonate, secondary amine, >N—H bend, C≡C terminal alkyne (monosubstituted), C≡C medial alkyne (disubstituted) and hydroxy, OH group at bandwidth peaks of 1760, 1650, 2140, 2190 and 3200 cm^{-1}, respectively. These new functional groups have resulted from the aggressive interaction between CO_2, KOH, and other volatile components during activation processes.

Fig. 3 shows the possible mechanism attraction between OXY molecules and the functional groups in LBWAC. The OXY molecules
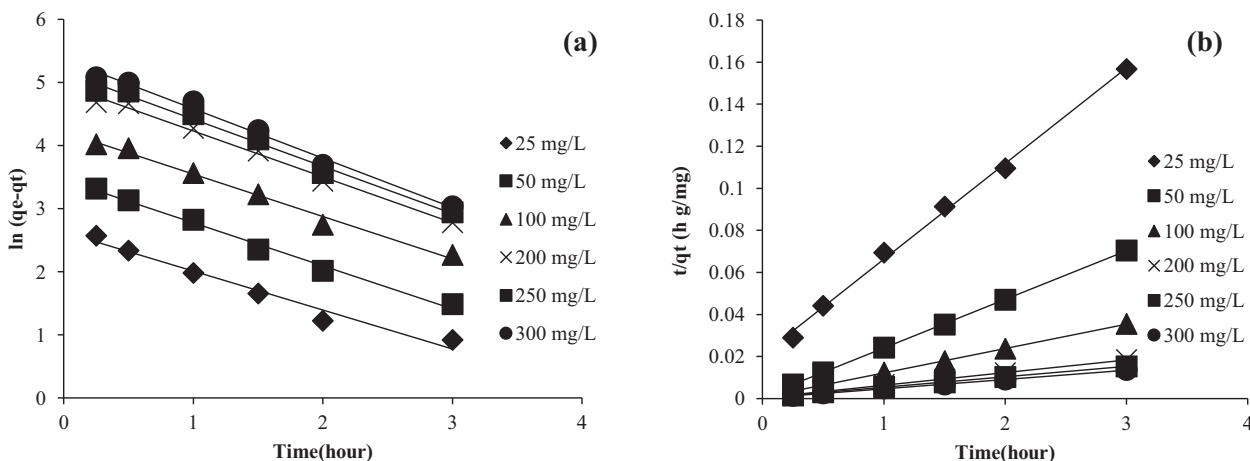
Fig. 10. Kinetic plots of (a) PFO and (b) PSO for OXY–LBWAC adsorption system at 30 °C (weight of LWBAC was 0.2 g, volume solution of 200 mL and original pH were used).

Table 4
Kinetic parameters for OXY–LBWAC adsorption system at 30 °C.

Starting OXY concentration (mg/L)	q_e, exp (mg/g)	Pseudo-first order (PFO)				Pseudo-second order (PSO)			
		q_e, cal (mg/g)	k_1 (min^{-1})	R^2	Error (%)	q_e, cal (mg/g)	k_2 (g mg^{-1} min^{-1})	R^2	Error (%)
	50	42.13	31.79	0.6826	0.9905	24.53	43.29	0.5929	0.9999	2.76
	100	82.71	68.27	0.6738	0.9886	17.47	86.21	0.2243	0.9998	4.22
	200	157.74	142.45	0.7281	0.992	9.69	166.67	0.0900	0.9994	5.66
	250	186.09	174.78	0.7462	0.9875	6.08	200.00	0.0625	0.9993	7.47
	300	212.79	214.22	0.7819	0.989	0.67	227.27	0.0645	0.9996	6.81
	Average				**0.9863**	**15.78**			**0.9992**	**4.74**
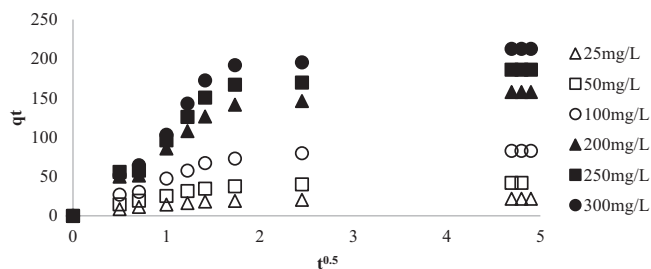
Fig. 11. Intraparticle plot for OXY-LBWAC adsorption systems at 30 °C (weight of LWBAC was 0.2 g, volume solution of 200 mL and original pH were used).

contain 9O and 2 N. These atoms are more electronegative and have the potential to form hydrogen bond with H atoms in terminal alkyne, primary amine, hydroxy and alkyl carbonate. Also, N atoms in primary amine, O atoms in hydroxy and alkyl carbonate have potential to form hydrogen bonds with H atoms in OXY molecules. These interactions had aided the adsorption of OXY onto LBWAC. Pham et al., (2019) also found hydrogen bond plays a major role in the adsorption of OXY onto alumina particles.

3.2. Adsorption equilibrium

3.2.1. Influence of contact time and OXY starting concentration

Fig. 4(a) and (b) provide the plot of OXY uptakes versus time at different starting concentrations and the plot of OXY percentage removal versus time at different starting concentrations, respectively. Based on Fig. 4(a), when OXY starting concentration increased from 25 to 300 mg/L, adsorption uptakes increased too from 21.65 to 212.79 mg/g. At higher starting concentrations, more OXY molecules are available in the solution to be adsorbed by LBWAC. It was also noticed that lower starting concentrations between 25 and 100 mg/L attained an equilibrium state faster at 6 h whereas higher starting concentrations between 200 and 300 mg/L achieved the same state at a longer time of 22 h. Based on Fig. 4(b), as the starting concentrations increased from 25 to 300 mg/L, OXY percentage removal decreased from 86.58 to 70.93%. At all starting concentrations studied, the number of active sites on LBWAC was constant. However, the quantity of OXY molecules was smaller at lower starting concentration, therefore, the adsorption process can complete faster, and the percentage removal was higher, and vice versa (Ahmad et al., 2021).

Table 5
Intraparticle diffusion parameters for OXY–LBWAC adsorption system at 30 °C.

Adsorption system	Adsorbates initial concentration (mg/L)	K_{p1} (mg/g h$^{1/2}$)	K_{p2} (mg/g h$^{1/2}$)	K_{p3} (mg/g h$^{1/2}$)	C_1	C_2	C_3	R_1^2	R_2^2	R_3^2
OXY-LBWAC	25	16.25	6.54	0.54	0.11	8.27	19.05	0.9968	0.9302	0.9948
	50	27.53	16.51	0.83	0.17	10.15	38.13	0.9974	0.9290	0.9948
	100	45.09	35.36	1.22	0.99	13.81	76.85	0.9672	0.9522	0.9948
	200	77.71	76.43	4.84	2.49	12.89	134.53	0.9331	0.9662	0.9948
	250	87.08	97.28	6.97	2.83	4.40	152.65	0.9314	0.9492	0.9948
	300	93.54	120.86	7.34	1.14	9.59	177.57	0.9898	0.9394	0.9948
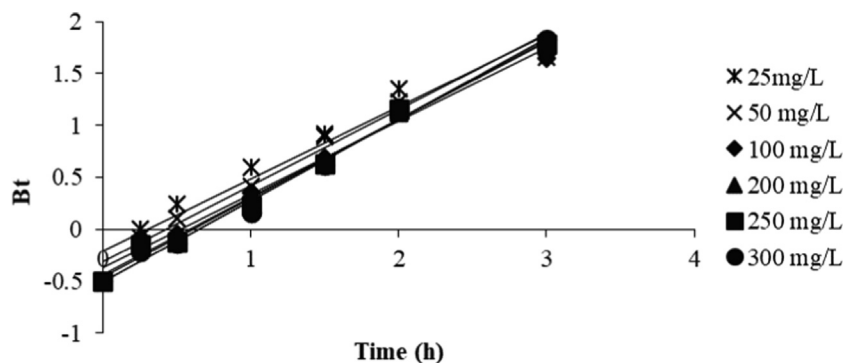
Fig. 12. Boyd plot for OXY-LBWAC adsorption systems at 30 °C (weight of LWBAC was 0.2 g, volume solution of 200 mL and original pH were used).

Mohamad Nasran Nasehir Khan, Mohamad Firdaus Mohamad Yusop, Muhamad Faizal Pakir Mohamed Latiff et al.

Arabian Journal of Chemistry 16 (2023) 105256

Table 6
Thermodynamic parameters for OXY-LBWAC adsorption system.

$\Delta H°$ (kJ/mol)	$\Delta S°$ (kJ/mol.K)	$\Delta G°$ (kJ/mol)			E_a (kJ/mol)
		303 K	318 K	333 K	
5.59	0.04	−5.73	−6.29	−6.85	20.01
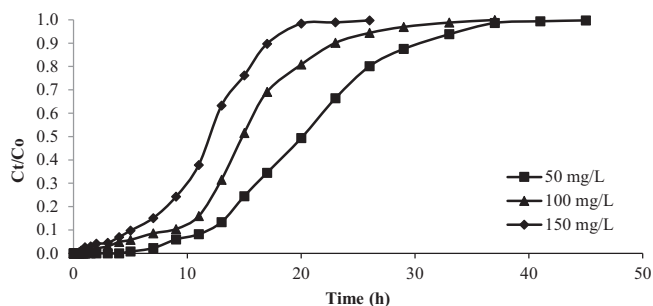
Fig. 13. Breakthrough curve for OXY-LBWAC at different influent starting concentration (flow rate = 10 mL/min and bed height = 2 cm).

3.2.2. Influence of solution temperature

Fig. 5 presents the plot that showcased the relationship between adsorption uptakes of OXY at different solution temperatures. It was observed that as the solution temperature increased from 30 to 60 °C, the adsorption uptakes of OXY also increased from 212.79 to 228.44 mg/g. This finding suggests that higher solution temperatures favoured the adsorption process of OXY, indicating an endothermic behaviour. Higher OXY uptakes were caused by the increasing of kinetic energy of OXY molecules at higher solution temperatures (Li et al., 2019, Başkan et al., 2022). OXY uptakes also favoured at higher solution temperatures when adsorbed by zeolite/Fe$_3$O$_4$ particles (Başkan et al., 2022) and metal hydroxides (Eniola et al., 2020).

3.2.3. Influence of solution pH

Fig. 6 shows the influence of solution pH on OXY uptakes. The lowest uptakes occurred at pH 2 of 46.05 mg/g. At pH 2, H$^+$ ions occur in excess amounts and became attracted to the electronegative O and N atoms in OXY molecules. This phenomenon reduced the number of hydrogen bonds between OXY molecules and LBWAC's surface (refers to Fig. 3). At pH 4 and 6, the number of H$^+$ ions reduced, therefore OXY uptakes increased to 49.53 and 53.95 mg/g, respectively. At pH 8, OH$^-$ ions existed in the solution and induced the surface of LBWAC to be negatively charged. These negatively charged surface attracted the electropositive H atoms in OXY molecule. This effect combined with the formation of hydrogen bonds between the OXY molecule and functional groups caused the OXY uptakes to increase to 59.76 mg/g. At pH 10, OXY uptakes increased to 61.45 mg/g due to increasing of OH$^-$ ions in solution. At pH 12, only a small increment occurred for OXY uptakes to be 63.22 mg/g. At this pH, the induced effect of OH$^-$

Fig. 14. Breakthrough curve for OXY- LBWAC at different flow rate (influent starting concentration = 100 mg/L and column bed height = 2 cm).

had reached its limit. Adding more OH$^-$ in the solution brings no more effect to the OXY uptakes.

3.3. Adsorption isotherm

Figs. 7, 8, and 9 present the isotherm plots of Langmuir, Freundlich, and Temkin models, whilst the isotherm parameters are summarized in Table 3. Adsorption of OXY onto LBWAC obeyed the Langmuir model due to the highest R^2 obtained of 0.9939. This indicated that OXY molecules developed a monolayer covering the surface of the LBWAC (García et al., 2018). The Langmuir maximum monolayer adsorption capacity, Q_m for OXY by LBWAC was found to be 344.83 mg/g. This value was higher as compared to the OXY-metal hydroxide adsorption system of 250.07 mg/g (Eniola et al., 2020), the OXY- zeolite/Fe$_3$O$_4$ adsorption system of 83.33 mg/g (Başkan et al., 2022). The heterogeneity factor, n_F, was determined to be 1.40. As this value falls within the range of 1 to 10, it indicates that the adsorption system studied is favourable (Firdaus et al., 2022).

3.4. Adsorption kinetic

The kinetic plots of PFO and PSO are shown in Fig. 10(a) and (b), respectively, while Table 4 shows the summary of kinetic parameters. The analysis revealed that the adsorption system exhibited the strongest adherence to the PSO kinetic model, as evidenced by the highest R^2 value of 0.9992 and a low error percentage of 4.74%. Adsorption of OXY onto hydroxyapatite (Harja and Ciobanu 2018) and alumina particles (Pham et al., 2019) were also best described by PSO kinetic model. Reaction rate, k_2 dropped from 0.0991 to 0.0645 g mg^{-1} min^{-1} as the OXY starting concentration increased from 25 to 300 mg/L. At higher starting OXY concentration, higher mass transfer driving force was developed, thus enhancing the adsorption process to be faster, and vice versa.

Fig. 11 provides the intraparticle diffusion plot while Table 5 shows the summary for intraparticle diffusion parameters. The lines depicted in Fig. 11 did not pass through the origin of the graph. Hence, it can be inferred that the rate-limiting step was

Table 7
Continuous bed column parameters for OXY-LBWAC system studied at different influent starting concentration (flow rate = 10 mL/min and bed height = 2 cm).

Inlet concentration, C_o (mg/L)	Mass of adsorbent (g)	Breakthrough point, T_b(h)	Exhaustion time, T_{ex} (h)	Total adsorption uptake, q_T (mg)	Maximum adsorption uptake, q_{max} (mg/g)
50	2.13	11	2940	906.60	425.63
100	3.47	7	2460	1470.00	423.63
150	3.58	5	1740	1498.80	418.65

Table 8
Continuous column parameters for OXY-LBWAC system studied at different influent flow rates (C_o = 100 mg/L and bed height = 2 cm).

Flow rate (mL/min)	Mass of adsorbent (g)	Breakthrough time, T_b	Exhaustion time, T_{ex} (h)	Total adsorption uptake, q_T (mg)	Maximum adsorption uptake, q_{max} (mg/g)
5	1.67	15	35	887.10	531.19
10	3.37	5	26	1446.00	429.08
15	2.7	2	17	790.20	292.67
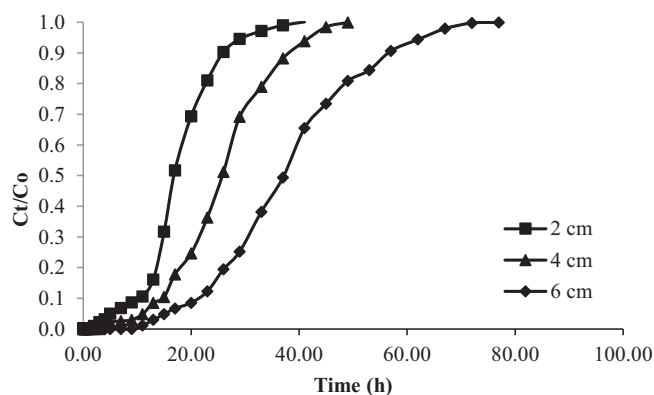
Fig. 15. Breakthrough curve for OXY- LBWAC at different column bed height (influent starting concentration = 100 mg/L and influent flow rate = 10 mL/min).

not solely governed by intraparticle diffusion (Björklund and Li 2017). Instead, the presence of multi-linear plots in Fig. 11 was observed, indicating the existence of three distinct mechanism pathways. The first region ($t^{0.5}$ = 0 to $t^{0.5}$ = 1) was predominantly influenced by film layer diffusion, characterized by electrical interactions between the outer surface of LBWAC and the OXY molecules (Sun et al., 2015). The second region ($t^{0.5}$ = 1 to $t^{0.5}$ = 2.5) corresponds to the slow adsorption stage, during which intraparticle diffusion emerged as the primary factor influencing the rate limiting step (Wang et al., 2015). The last stage ($t^{0.5}$ = 2.5 to $t^{0.5}$ = 5) signifies the attainment of the equilibrium stage, where the number of adsorbate molecules in the solution becomes minimal. During this phase, the intraparticle diffusion process gradually decelerates (Wang et al., 2010).

Fig. 12 presents the Boyd plots for the OXY-LBWAC adsorption system at 30 °C. It was observed that the rate-limiting step for all the OXY starting concentrations was governed by film diffusion. This conclusion was drawn based on the fact that these plots did not pass through the origin (Garba and Rahim 2016).

3.5. Adsorption thermodynamic

Table 6 summarizes the thermodynamic parameters for the OXY-LBWAC adsorption system. The $\Delta H°$ for the OXY-LBWAC adsorption system was found to be 5.59 kJ/mol. The positive sign of $\Delta H°$ value signified the endothermic nature of the adsorption

systems studied where higher adsorbate uptakes occurred at higher solution temperatures. This discovery was consistent with the finding in Section 3.2.2. The $\Delta S°$ was found to be 0.04 kJ/mol. K, and the positive value of this parameter implied the randomness level at solid–liquid interface had increased. The $\Delta G°$ values were between −5.73 and −6.85 kJ/mol. The negative sign of this parameter indicates that the adsorption process was spontaneous in nature. The E_a value was 20.01 kJ/mol and since it was below 42 kJ/mol, the adsorption process was dominated by physisorption (Hao et al., 2020).

3.6. Continuous adsorption in bed column

3.6.1. Influence of influent starting concentration
The breakthrough curve for the OXY-LBWAC adsorption system under the influence of different influent starting concentrations is given in Fig. 13. The parameters extracted from Fig. 13 were tabulated in Table 7. From Table 7, when the influent starting concentration increased from 50 to 150 mg/L, the breakthrough time, T_b, and the exhaustion time, T_{ex} had reduced from 11 to 5 h and 49 to 29 h, respectively. At lower influent starting concentrations, the number of OXY molecules to be adsorbed by LBWAC was lower. Therefore, a longer time was taken for OXY molecules to breakthrough the bed column and appeared in the effluent. Similarly, a longer time was needed by lower influent starting concentration to achieve T_{ex}.

3.6.2. Influence of influent flow rate
The breakthrough curve for the OXY-LBWAC adsorption system under the influence of different influent flow rates is given in Fig. 14. The parameters gathered from Fig. 14 were presented in Table 8. As the influent flow rate increased from 5 to 15 mL/min, the T_b and T_{ex} declined from 15 h to 2 h and 35 h to 17 h, respectively. Hence, it concludes that a low influent flow rate prolonged T_b and T_{ex}. At a high influent flow rate, the contact time between OXY molecules and the surface of LBWAC was limited, causing the OXY molecules to exit the bed column even before the adsorption process is complete. In addition, higher flow rates were found to cause increased turbulence, resulting in weak mass transfer and limited contact between OXY and LBWAC. Consequently, this led to poor adsorbate removal efficiency (Dwivedi et al., 2008).

3.6.3. Influence of bed column height
The breakthrough curve for the OXY-LBWAC adsorption system under the influence of different bed column heights is given in

Table 9
Continuous column parameters for OXY-LBWAC system studied at different column bed height (C_o = 100 mg/L and flow rate = 10 mL/min).

Bed height (cm)	Mass of adsorbent (g)	Breakthrough time, T_b(h)	Exhaustion time, T_{ex} (h)	Total adsorption uptake, q_T (mg)	Maximum adsorption uptake, q_{max} (mg/g)
2	3.37	5	26	1343.40	398.63
4	3.78	11	37	1991.40	526.82
6	4.92	15	57	3299.40	670.60

Table 10
Parameters obtained from the different models.

Adams-Bohart model		
k_A (L/mg min)	N_o (mg/L)	R^2
0.00160	7370.08	0.7790
Thomas model		
k_{TH} (mL/min mg)	q_{TH} (mg/g)	R^2
0.0106	5181.73	0.9538
Yoon-Nelson model		

$t_{0.5}$ (min)	τ (min)	k_Y (1/min)	R^2
1011	1188	0.0050	0.9380

Fig. 15. The parameters obtained from Fig. 15 were showed in Table 9. As the bed height in the column increased, T_b and T_{ex} increased from 5 h to 15 h and 26 h to 57 h, respectively. As the bed height increased, more surface area became accessible for the adsorption process to occur. Consequently, it took more time for the LBWAC to be exhausted (Kazemi et al., 2016). Moreover, higher bed height resulted in a longer contact time between OXY and LBWAC, thus improving the adsorption process. This justification supported the finding that higher maximum adsorption uptake, q_{max} was achieved at the highest column bed height.

3.7. Breakthrough modelling

The data from the continuous bed column study were fitted to three models namely Adams-Bohart, Thomas, and Yoon-Nelson with constant. The parameters for these models were tabulated in Table 10. According to Table 10, the Adams-Bohart model exhibits the lowest R^2 values for OXY adsorption, specifically measuring 0.7790. This suggests a weak correlation between the Adams-Bohart model and the experimental data, indicating that the model poorly represents the adsorption process. Consequently, it can be inferred that intraparticle diffusion is not the limiting factor in the rate of adsorption. This conclusion aligns with the findings from the investigation of the batch adsorption mechanism, which indicates that film diffusion serves as the rate-limiting phase (Section 3.4). From Table 10, Thomas model shows very good correlations for breakthrough data with R^2 values of 0.9538 for OXY-LBWAC adsorption system. The Thomas model assumes that the adsorption process follows a PSO kinetic model. This was aligned with the finding obtained in batch kinetic study (Section 3.4). From Table 10, the R^2 of Yoon-Nelson model was found to be relatively high too of 0.9380. This model predicts the 50% breakthrough time ($t^{0.5}$) to be 1011 m. This value is relatively accurate with the actual $t^{0.5}$ of 900 m (error 10.98%).

4. Conclusion

LBWAC was successfully produced using KOH and CO_2 activation, combined with microwave irradiation. LBWAC effectively removed OXY, with a maximum adsorption capacity, Q_m of 344.83 mg/g. LBWAC exhibited a high BET surface area (973.21 m^2/g), mesopores surface area (842.18 m^2/g), and total pore volume (0.3911 cm^3/g). In the equilibrium study, as the initial concentration of OXY increased from 25 to 300 mg/L, the adsorption uptake increased while the percentage removal decreased. The highest OXY removal was observed at pH 12 (63.22 mg/g), and a solution temperature of 60 °C (228.44 mg/g). The adsorption data of AMOX-LBWAC exhibited the best fit with the Langmuir isotherm model and PSO kinetic model. The Boyd plot analysis indicated that film diffusion was the rate-determining step in the adsorption process. The enhancement of the adsorption process was attributed to the formation of hydrogen bonds between OXY molecules and specific functional groups present in LBWAC, including primary amine, hydroxy, alkyl carbonate, and terminal alkyne groups. The thermodynamic analysis indicated that the adsorption process is characterized as endothermic, spontaneous, and governed by physical interactions. In bed column studies, the highest values for T_b, T_{ex}, and q_{max} were obtained at 50 mg/L, 5 mL/min, and 6 cm of OXY influent starting concentration, influent flow rate and LBWAC bed height, respectively. The continuous adsorption data showed the best fit with the Thomas model. The LBWAC produced demonstrated favourable characteristics as an adsorbent, making it suitable for utilization in large-scale antibiotic treatment systems operating in a continuous mode.

Declaration of Competing Interest

The authors declare that they have no known competing financial interests or personal relationships that could have appeared to influence the work reported in this paper.

Acknowledgments

References

Achmad, A., Kassim, J., Suan, T.K., et al., 2012. Equilibrium, kinetic and thermodynamic studies on the adsorption of direct dye onto a novel green adsorbent developed from Uncaria gambir extract. J. Phys. Sci. 23, 1–13.

Ahmad, M.A., Eusoff, M.A., Oladoye, P.O., et al., 2020b. Statistical optimization of Remazol Brilliant Blue R dye adsorption onto activated carbon prepared from pomegranate fruit peel. Chem. Data Collect. 28,. https://doi.org/10.1016/j.cdc.2020.100426 100426.

Ahmad, A., Jini, D., Aravind, M., et al., 2020a. A novel study on synthesis of egg shell based activated carbon for degradation of methylene blue via photocatalysis. Arab. J. Chem. 13, 8717–8722. https://doi.org/10.1016/j.arabjc.2020.10.002.

Ahmad, M.A., Yusop, M.F.M., Awang, S., et al., 2021. Carbonization of sludge biomass of water treatment plant using continuous screw type conveyer pyrolyzer for methylene blue removal. IOP Conf. Ser.: Earth Environ. Sci. 765,. https://doi.org/10.1088/1755-1315/765/1/012112 012112.

Ajay, K.M., Dinesh, M.N., Byatarayappa, G., et al., 2021. Electrochemical investigations on low cost KOH activated carbon derived from orange-peel and polyaniline for hybrid supercapacitors. Inorg. Chem. Commun. 127,. https://doi.org/10.1016/j.inoche.2021.108523 108523.

Alam, M.G., Danish, M., Alanazi, A.M., et al., 2023. Response surface methodology approach of phenol removal study using high-quality activated carbon derived from H_3PO_4 activation of Acacia mangium wood. Diam. Relat. Mater. 132,. https://doi.org/10.1016/j.diamond.2022.109632 109632.

Amran, F., Zainuddin, N.F., Ahmad Zaini, M.A., 2021. Two-stage batch adsorber design for methylene blue removal by coconut shell activated carbon. Malaysian J. Fundamental Appl. Sci. 17, 768–775. https://doi.org/10.11113/MJFAS.V17N6.2303.

Arshad, S.H.M., Ngadi, N., Wong, S., et al., 2019. Optimization of phenol adsorption onto biochar from oil palm empty fruit bunch (EFB). Malaysian J. Fundamental Appl. Sci. 15, 1–5. https://doi.org/10.11113/mjfas.v15n2019.1199.

Askaruly, K., Korobeinyk, A.V., Azat, S., et al., 2023. The electrochemical behavior of silica and activated carbon materials derived from the rice husk waste for li-ion cells. Diam. Relat. Mater. 133,. https://doi.org/10.1016/j.diamond.2023.109759 109759.

Bai, X., Acharya, K., 2016. Removal of trimethoprim, sulfamethoxazole, and triclosan by the green alga Nannochloris sp. J. Hazard. Mater. 315, 70–75. https://doi.org/10.1016/j.jhazmat.2016.04.067.

Baruah, M., Ezung, S.L., Sharma, S., et al., 2022. Synthesis and characterization of Ni-doped TiO_2 activated carbon nanocomposite for the photocatalytic degradation of anthracene. Inorg. Chem. Commun. 144,. https://doi.org/10.1016/j.inoche.2022.109905 109905.

Başkan, G., Açıkel, Ü., Levent, M., 2022. Investigation of adsorption properties of oxytetracycline hydrochloride on magnetic zeolite/Fe_3O_4 particles. Adv. Powder Technol. 33,. https://doi.org/10.1016/j.apt.2022.103600 103600.

Björklund, K., Li, L.Y., 2017. Adsorption of organic stormwater pollutants onto activated carbon from sewage sludge. J. Environ. Manage. 197, 490–497. https://doi.org/10.1016/j.jenvman.2017.04.011.

Borghei, S.A., Zare, M.H., Ahmadi, M., et al., 2021. Synthesis of multi-application activated carbon from oak seeds by KOH activation for methylene blue adsorption and electrochemical supercapacitor electrode. Arab. J. Chem. 14,. https://doi.org/10.1016/j.arabjc.2020.102958 102958.

Mohamad Nasran Nasehir Khan, Mohamad Firdaus Mohamad Yusop, Muhamad Faizal Pakir Mohamed Latiff et al.

Arabian Journal of Chemistry 16 (2023) 105256

Boyd, G.E., Schubert, J., Adamson, A.W., 1947. The exchange adsorption of ions from aqueous solutions by organic zeolites. Ion-exchange equilibria. J. Am. Chem. Soc. 69, 2818–2829. https://doi.org/10.1021/ja01203a064.

Bumajdad, A., Hasila, P., 2023. Surface modification of date palm activated carbonaceous materials for heavy metal removal and CO_2 adsorption. Arab. J. Chem. 16,. https://doi.org/10.1016/j.arabjc.2022.104403 104403.

Conde-Cid, M., Ferreira-Coelho, G., Núñez-Delgado, A., et al., 2019. Competitive adsorption of tetracycline, oxytetracycline and chlortetracycline on soils with different pH value and organic matter content. Environ. Res. 178. https://doi.org/10.1016/j.envres.2019.108669.

Cuerda-Correa, E.M., Alexandre-Franco, M.F., Fernández-González, C., 2020. Advanced oxidation processes for the removal of antibiotics from water. An overview. Water (Switzerland) 12. https://doi.org/10.3390/w12010102.

Du, C., Zhang, Z., Yu, G., et al., 2021. A review of metal organic framework (MOFs)-based materials for antibiotics removal via adsorption and photocatalysis. Chemosphere 272. https://doi.org/10.1016/j.chemosphere.2020.129501.

Dwivedi, C.P., Sahu, J.N., Mohanty, C.R., et al., 2008. Column performance of granular activated carbon packed bed for Pb(II) removal. J. Hazard. Mater. 156, 596–603. https://doi.org/10.1016/j.jhazmat.2007.12.097.

Eniola, J.O., Kumar, R., Al-Rashdi, A.A., et al., 2020. Hydrothermal synthesis of structurally variable binary CuAl, MnAl and ternary CuMnAl hydroxides for oxytetracycline antibiotic adsorption. J. Environ. Chem. Eng. 8,. https://doi.org/10.1016/j.jece.2019.103535 103535.

Ferrando, L., Matamoros, V., 2020. Attenuation of nitrates, antibiotics and pesticides from groundwater using immobilised microalgae-based systems. Sci. Total Environ. 703. https://doi.org/10.1016/j.scitotenv.2019.134740.

Firdaus, M.Y.M., Aziz, A., Azmier Ahmad, M., 2022. Conversion of teak wood waste into microwave-irradiated activated carbon for cationic methylene blue dye removal: optimization and batch studies. Arab. J. Chem. 15,. https://doi.org/10.1016/j.arabjc.2022.104081 104081.

Freundlich, H., 1906. Over the adsorption in solution (1906) Z. Phys. Chem. 57, 358–471.

Garba, Z.N., Rahim, A.A., 2016. Evaluation of optimal activated carbon from an agricultural waste for the removal of para-chlorophenol and 2,4-dichlorophenol. Process Saf. Environ. Prot. 102, 54–63. https://doi.org/10.1016/j.psep.2016.02.006.

García, J.R., Sedran, U., Zaini, M.A.A., et al., 2018. Preparation, characterization, and dye removal study of activated carbon prepared from palm kernel shell. Environ. Sci. Pollut. Res. 25, 5076–5085. https://doi.org/10.1007/s11356-017-8975-8.

Gojkovic, Z., Lindberg, R.H., Tysklind, M., et al., 2019. Northern green algae have the capacity to remove active pharmaceutical ingredients. Ecotoxicol. Environ. Saf. 170, 644–656. https://doi.org/10.1016/j.ecoenv.2018.12.032.

Hao, L., Gao, W., Yan, S., et al., 2020. Functionalized diatomite/oyster shell powder doped electrospun polyacrylonitrile submicron fiber as a high-efficiency adsorbent for removing methylene blue from aqueous solution: thermodynamics, kinetics and isotherms. J. Mol. Liq. 298,. https://doi.org/10.1016/j.molliq.2019.112022 112022.

Harja, M., Ciobanu, G., 2018. Studies on adsorption of oxytetracycline from aqueous solutions onto hydroxyapatite. Sci. Total Environ. 628–629, 36–43. https://doi.org/10.1016/j.scitotenv.2018.02.027.

He, S., Sun, J., Jin, X., et al., 2023. Adsorption enhancement of Congo red dye from wastewater based on edamame shell originated activated carbon by the cations: experimental and theoretical studies. Diam. Relat. Mater. 136,. https://doi.org/10.1016/j.diamond.2023.109930 109930.

Ho, Y.S., McKay, G., 1998. Sorption of dye from aqueous solution by peat. Chem. Eng. J. 70, 115–124. https://doi.org/10.1016/S0923-0467(98)00076-1.

Jawad, A.H., Saber, S.E.M., Abdulhameed, A.S., et al., 2022. Mesoporous activated carbon from mangosteen (Garcinia mangostana) peels by H_3PO_4 assisted microwave: Optimization, characterization, and adsorption mechanism for methylene blue dye removal. Diam. Relat. Mater. 129,. https://doi.org/10.1016/j.diamond.2022.109389 109389.

Juengchareonpoon, K., Boonamnuayvitaya, V., Wanichpongpan, P., 2019. Kinetics and isotherms of oxytetracycline adsorption on β-cyclodextrin/carboxymethylcellulose hydrogel films. Aquac. Res. 50, 3412–3419. https://doi.org/10.1111/are.14299.

Karakehya, N., 2023. Effects of one-step and two-step KOH activation method on the properties and supercapacitor performance of highly porous activated carbons prepared from Lycopodium clavatum spores. Diam. Relat. Mater. 135,. https://doi.org/10.1016/j.diamond.2023.109873 109873.

Kazemi, F., Younesi, H., Ghoreyshi, A.A., et al., 2016. Thiol-incorporated activated carbon derived from fir wood sawdust as an efficient adsorbent for the removal of mercury ion: Batch and fixed-bed column studies. Process Saf. Environ. Prot. 100, 22–35. https://doi.org/10.1016/j.psep.2015.12.006.

Khan, A., Huo, Y., Qu, Z., et al., 2021. A facile calcination conversion of groundwater treatment sludge (GTS) as magnetic adsorbent for oxytetracycline adsorption. Sci. Rep. 11, 5276. https://doi.org/10.1038/s41598-021-84231-8.

Kovalakova, P., Cizmas, L., McDonald, T.J., et al., 2020. Occurrence and toxicity of antibiotics in the aquatic environment: a review. Chemosphere 251,. https://doi.org/10.1016/j.chemosphere.2020.126351 126351.

Lagergren, S.K., 1898. About the theory of so-called adsorption of soluble substances. Sven. Vetenskapsakad. Handingarl. 24, 1–39.

Langmuir, I., 1918. The adsorption of gases on plane surfaces of glass, mica and platinum. J. Am. Chem. Soc. 40, 1361–1403. https://doi.org/10.1021/ja02242a004.

Leng, L., Wei, L., Xiong, Q., et al., 2020. Use of microalgae based technology for the removal of antibiotics from wastewater: a review. Chemosphere 238. https://doi.org/10.1016/j.chemosphere.2019.124680.

Li, W., Cao, J., Xiong, W., et al., 2020. In-situ growing of metal-organic frameworks on three-dimensional iron network as an efficient adsorbent for antibiotics removal. Chem. Eng. J. 392. https://doi.org/10.1016/j.cej.2020.124844.

Li, N., Zhou, L., Jin, X., et al., 2019. Simultaneous removal of tetracycline and oxytetracycline antibiotics from wastewater using a ZIF-8 metal organic-framework. J. Hazard. Mater. 366, 563–572. https://doi.org/10.1016/j.jhazmat.2018.12.047.

Lima, E.C., Hosseini-Bandegharaei, A., Moreno-Piraján, J.C., et al., 2019. A critical review of the estimation of the thermodynamic parameters on adsorption equilibria. Wrong use of equilibrium constant in the Van't Hoof equation for calculation of thermodynamic parameters of adsorption. J. Mol. Liq. 273, 425–434. https://doi.org/10.1016/j.molliq.2018.10.048.

Lin, C.S., Ibrahim, N., Ahmad, N., et al., 2021. Nitric oxide removal by zinc chloride activated oil palm empty fruit bunch fibre. Malaysian J. Fundamental Appl. Sci. 17, 84–89. https://doi.org/10.11113/MJFAS.V17N1.2171.

Liu, Z., Pu, C., Du, X., et al., 2023. Combined effects of pore structure and surface chemistry on water vapor adsorption characteristics of coal: equilibrium, thermodynamic and kinetic studies. Arab. J. Chem. 16,. https://doi.org/10.1016/j.arabjc.2023.104790 104790.

Lopes, G.K.P., Zanella, H.G., Spessato, L., et al., 2021. Steam-activated carbon from malt bagasse: optimization of preparation conditions and adsorption studies of sunset yellow food dye. Arab. J. Chem. 14,. https://doi.org/10.1016/j.arabjc.2021.103001 103001.

Mawhinney, D.B., Yates, J.T., 2001. FTIR study of the oxidation of amorphous carbon by ozone at 300 K — Direct COOH formation. Carbon 39, 1167–1173. https://doi.org/10.1016/S0008-6223(00)00238-4.

Mohamad Yusop, M.F., Abdullah, A.Z., Ahmad, M.A., 2023a. Malachite green dye adsorption by jackfruit based activated carbon: Optimization, mass transfer simulation and surface area prediction. Diam. Relat. Mater. 136,. https://doi.org/10.1016/j.diamond.2023.109991 109991.

Mohamad Yusop, M.F., Nasehir Khan, M.N., Zakaria, R., et al., 2023b. Mass transfer simulation on remazol brilliant blue R dye adsorption by optimized teak wood Based activated carbon. Arab. J. Chem. 16,. https://doi.org/10.1016/j.arabjc.2023.104780 104780.

Mohamad Yusop, M.F., Tamar Jaya, M.A., Idris, I., et al., 2023c. Optimization and mass transfer simulation of remazol brilliant blue R dye adsorption onto meranti wood based activated carbon. Arab. J. Chem. 16,. https://doi.org/10.1016/j.arabjc.2023.104683 104683.

Moradi, H., Azizpour, H., Bahmanyar, H., et al., 2020. Molecular dynamics simulation of H2S adsorption behavior on the surface of activated carbon. Inorg. Chem. Commun. 118,. https://doi.org/10.1016/j.inoche.2020.108048 108048.

Nguyen, D.T.C., Vo, D.-V.-N., Nguyen, C.N.Q., et al., 2021. Box-Behnken design, kinetic, and isotherm models for oxytetracycline adsorption onto Co-based ZIF-67. Appl. Nanosci. 11, 2347–2359. https://doi.org/10.1007/s13204-021-01954-w.

Nkoh, J.N., Oderinde, O., Etafo, N.O., et al., 2023. Recent perspective of antibiotics remediation: a review of the principles, mechanisms, and chemistry controlling remediation from aqueous media. Sci. Total Environ. 881,. https://doi.org/10.1016/j.scitotenv.2023.163469 163469.

Nor, N.M., Chung, L.L., Mohamed, A.R., 2021. Nitrogen tailored activated carbon via microwave synthesis method for high removal of hydrogen sulfide. Malaysian J. Fundamental Appl. Sci. 17, 794–804. https://doi.org/10.11113/MJFAS.V17N6.2319.

Norouzi, S., Heidari, M., Alipour, V., et al., 2018. Preparation, characterization and Cr (VI) adsorption evaluation of NaOH-activated carbon produced from Date Press Cake; an agro-industrial waste. Bioresour. Technol. 258, 48–56. https://doi.org/10.1016/j.biortech.2018.02.106.

Nur, L., Paharudin, H., Nur, S., et al., 2014. Determination of phenolic compounds from Tabebuia Rosea (USIM Sakura) trees extracted oil using fourier-transform infrared spectroscopy. Proceeding Insan Junior Researchers Int. Conf., 73–81

Oyekanmi, A.A., Latiff, A.A.A., Daud, Z., et al., 2019. Batch adsorption of activated coconut shell for the removal of zinc from palm oil mill effluent. Malaysian J. Fundamental Appl. Sci. 15, 708–711. https://doi.org/10.11113/mjfas.v15n5.1444.

Pham, T.D., Tran, T.T., Le, V.A., et al., 2019. Adsorption characteristics of molecular oxytetracycline onto alumina particles: the role of surface modification with an anionic surfactant. J. Mol. Liq. 287,. https://doi.org/10.1016/j.molliq.2019.110900 110900.

Rosli, N.A., Ahmad, M.A., Noh, T.U., 2023. Nature's waste turned savior: optimizing pineapple peel–based activated carbon for effective Remazol Brilliant Violet dye adsorption using response surface methodology. Inorg. Chem. Commun. 153,. https://doi.org/10.1016/j.inoche.2023.110844 110844.

Said, B., Bacha, O., Rahmani, Y., et al., 2023. Activated carbon prepared by hydrothermal pretreatment-assisted chemical activation of date seeds for supercapacitor application. Inorg. Chem. Commun. 155,. https://doi.org/10.1016/j.inoche.2023.111012 111012.

Saka, C., Teğin, İ., Kahvecioğlu, K., 2023. Sulphur-doped carbon particles from almond shells as cheap adsorbent for efficient Cd(II) adsorption. Diam. Relat. Mater. 131,. https://doi.org/10.1016/j.diamond.2022.109542 109542.

Senol-Arslan, D., Gül, A., Uzal, N., et al., 2022. Ni-Zn metal-organic framework based membranes for rejection of Pb(II) ions. Inorg. Chem. Commun. 146,. https://doi.org/10.1016/j.inoche.2022.110084 110084.

Sun, X., Cheng, P., Wang, H., et al., 2015. Activation of graphene aerogel with phosphoric acid for enhanced electrocapacitive performance. Carbon 92, 1–10. https://doi.org/10.1016/j.carbon.2015.02.052.

Tempkin, M., Pyzhev, V., 1940. Kinetics of ammonia synthesis on promoted iron catalyst. J. Acta Phys. Chim. USSR. 12, 327.

Tiwari, G., Rekha Devi, R., Mahanta, S.P., et al., 2023. Copper oxide nanoparticles modified activated carbon nanocomposite towards removal of tetracycline from waste water. Inorg. Chem. Commun. 152,. https://doi.org/10.1016/j.inoche.2023.110687 110687.

Van Boeckel, T.P., Brower, C., Gilbert, M., et al., 2015. Global trends in antimicrobial use in food animals. Proc. Natl. Acad. Sci. U.S.A. 112, 5649–5654. https://doi.org/10.1073/pnas.1503141112.

Wang, P., Ma, Q., Hu, D., et al., 2015. Removal of Reactive Blue 21 onto magnetic chitosan microparticles functionalized with polyamidoamine dendrimers. React. Funct. Polym. 91–92, 43–50. https://doi.org/10.1016/j.reactfunctpolym.2015.04.007.

Wang, M., Shen, J., Xu, X., et al., 2023. Biochar as an enhancer of the stability, mesoporous structure and oxytetracycline adsorption capacity of ferrihydrite: role of the silicon component. Sci. Total Environ. 875,. https://doi.org/10.1016/j.scitotenv.2023.162652 162652.

Wang, L., Zhang, J., Zhao, R., et al., 2010. Adsorption of basic dyes on activated carbon prepared from Polygonum orientale Linn: equilibrium, kinetic and thermodynamic studies. Desalination 254, 68–74. https://doi.org/10.1016/j.desal.2009.12.012.

Xiong, Q., Hu, L.X., Liu, Y.S., et al., 2021. Microalgae-based technology for antibiotics removal: from mechanisms to application of innovational hybrid systems. Environ. Int. 155. https://doi.org/10.1016/j.envint.2021.106594.

Xu, Z., Chen, J., Zhang, X., et al., 2019. Template-free preparation of nitrogen-doped activated carbon with porous architecture for high-performance supercapacitors. Microporous Mesoporous Mater. 276, 280–291. https://doi.org/10.1016/j.micromeso.2018.09.023.

Yusop, M.F.M., Ahmad, M.A., Rosli, N.A., et al., 2021. Scavenging malachite green dye from aqueous solution using durian peel based activated carbon. Malaysian J. Fundamental Appl. Sci. 17, 95–103. https://doi.org/10.11113/MJFAS.V17N1.2173.

Yusop, M.F.M., Jaya, E.M.J., Ahmad, M.A., 2022a. Single-stage microwave assisted coconut shell based activated carbon for removal of Zn(II) ions from aqueous solution – Optimization and batch studies. Arab. J. Chem. 15,. https://doi.org/10.1016/j.arabjc.2022.104011 104011.

Yusop, M.F.M., Mohd Johan Jaya, E., Mohd Din, A.T., et al., 2022b. Single-Stage optimized microwave-induced activated carbon from coconut shell for cadmium adsorption. Chem. Eng. Technol. 45, 1943–1951. https://doi.org/10.1002/ceat.202200051.

Zayed, A.M., Metwally, B.S., Masoud, M.A., et al., 2023. Facile synthesis of eco-friendly activated carbon from leaves of sugar beet waste as a superior nonconventional adsorbent for anionic and cationic dyes from aqueous solutions. Arab. J. Chem. 16,. https://doi.org/10.1016/j.arabjc.2023.104900 104900.

Zhan, H., Wang, Y., Mi, X., et al., 2020. Effect of graphitic carbon nitride powders on adsorption removal of antibiotic resistance genes from water. Chin. Chem. Lett. 31, 2843–2848. https://doi.org/10.1016/j.cclet.2020.08.015.

Zhang, Z., He, H., Han, T., et al., 2023. Soil oxytetracycline alters the effects of phosphate fertilisation and Bacillus amyloliquefaciens on the bacterial community of Medicago sativa rhizosphere. Appl. Soil Ecol. 187,. https://doi.org/10.1016/j.apsoil.2023.104861 104861.

Zhao, R., Feng, J., Liu, J., et al., 2019. Deciphering of microbial community and antibiotic resistance genes in activated sludge reactors under high selective pressure of different antibiotics. Water Res. 151, 388–402. https://doi.org/10.1016/j.watres.2018.12.034.

Zhou, Q., Wu, Y., Chen, H., et al., 2022. Preparation of Quercus mongolica leaf-derived porous carbon with a large specific surface area for highly effective removal of dye and antibiotic from water. Arab. J. Chem. 15,. https://doi.org/10.1016/j.arabjc.2022.104031 104031.